Research Article

Seong-Hwang Kim, Yinhang Zhang, Jong-Hoon Lee, Seul-Yi Lee, Yeong-Hun Kim, Kyong Yop Rhee*, and Soo-Jin Park*

A study on interfacial behaviors of epoxy/graphene oxide derived from pitch-based graphite fibers

https://doi.org/10.1515/ntrev-2021-0111
received July 16, 2021; accepted September 25, 2021

Abstract: Graphene oxide (GO) is a versatile material with inherent unique properties that can be used in a wide range of applications. GO is produced from graphitic materials including graphite, and its properties can depend on the nature of stacking in the graphene structures. In this study, GO was prepared from pitch-based graphite fibers *via* the modified Hummer's method and subsequently incorporated into an epoxy matrix to obtain graphene-loaded nanocomposites (EP/GO). Presented experimental results revealed that the addition of 0.6 wt% GO yielded an ~110% increase in the fracture toughness. The corresponding fracture energies as well as the flexural strengths and flexural modulus exhibited similar trends to the fracture toughness. The thermophysical properties of the EP/GO, to further demonstrate the reinforcing effectiveness of GO, were also observed. Collectively, these results indicate that GO investigated in the study can be a viable reinforcement candidate to develop next-generation nanocomposites with multifunctional properties.

Keywords: polymer-matrix composites, physical properties, wettability, fracture toughness

*** Corresponding author: Kyong Yop Rhee,** Department of Mechanical Engineering, College of Engineering, Kyung Hee University, Yongin, 17104, Republic of Korea, e-mail: rheeky@khu.ac.kr, tel: +82-31-201-2565; fax: +82-31-202-6693
*** Corresponding author: Soo-Jin Park,** Department of Chemistry, Inha University, 100 Inharo, Incheon 22212, Republic of Korea, e-mail: sjpark@inha.ac.kr, tel: +82-32-876-7234; fax: +82-32-860-8438
Seong-Hwang Kim, Yinhang Zhang, Jong-Hoon Lee, Yeong-Hun Kim: Department of Chemistry, Inha University, 100 Inharo, Incheon 22212, Republic of Korea
Seul-Yi Lee: Department of Chemistry, Inha University, 100 Inharo, Incheon 22212, Republic of Korea; Department of Mechanical Engineering and Institute for Critical Technology and Applied Science, Virginia Tech, Blacksburg, VA 24061, United States of America, e-mail: leesy@vt.edu

1 Introduction

Graphene-based materials, which contain a two-dimensional (2-D) single layer of carbon atoms arranged in a hexagonal lattice, have been widely investigated and commercialized because they are highly ordered, and they offer strong chemical resistance, large specific surface area ($2{,}630\ m^2\ g^{-1}$), high Young's modulus (1 TPa), high thermal conductivity ($5{,}000\ W\ m^{-1}\ K^{-1}$), and high electron mobility ($2.5 \times 10^5\ cm^2\ V^{-1}\ s^{-1}$) [1–7].

Many academic and industrial researchers are struggling in manufacturing graphene with high quality and large quantities, which is divided into two categories: one is the bottom-up method that synthesizes from hydrocarbon sources using chemical vapor deposition for single or a few layers with the minimum defect area [8,9]. This method cannot be used for most applications that require graphene in large quantities. The other is the top-down method that applies chemical and/or mechanical exfoliation of graphite, which is much advantageous to produce 2-D graphene oxide (GO) in a scalable manner. In particular, GO produced by the top-down method has attracted increasing attention as a nanofiller for polymer-based nanocomposites [10–12].

Until now, it was considered that graphite (synthetic or natural) is the primary source for mass production of GO or reduced GO using the top-down method. Jiao *et al.* reported that GOs synthesized from different types of natural graphite show a remarkable difference in the crystalline morphologies, chemical properties, *etc.* because of different graphitization degree [13]. Understanding the characteristics of precursors and controlling parameters such as medium and temperature during the synthesis process is crucial to obtain GO with desirable properties for use in a wide range of applications [14–17].

Along with these, other sp^2-carbon sources are widely used for GO production, such as graphite fibers (GFs) [18], carbon nanotubes [19], coal [20], and biomass [21]. Among

them, GFs have abundant crystalline graphite with a high carbon content of more than 99%. This is because they are manufactured by the graphitization process at approximately 3,000°C. GFs are thus extensively used in applications that require high strength and high modulus, including applications in the railways and the automotive, aerospace, drilling, and consumer product industries [22–27]. GFs with considerable amounts of 2-D conjugated sp^2 domains are acceptable, which can be converted to graphene and/or graphene derivatives for mass production [18,28,29].

In this study, GO was prepared from pitch-based GFs using a typical oxidation and subsequent exfoliation process, called the Hummer's method, and the chemical and morphological properties of GO were investigated. Moreover, GO-incorporated epoxy (EP/GO) nanocomposites as a function of GO loading amount were fabricated to investigate the interfacial interactions between GO and epoxy matrix. The present study aimed concretely at evaluating the effects of GO on the interfacial properties and mechanical properties (*e.g.*, surface free energy, interfacial adhesion, fracture toughness, flexural strength, and flexural modulus) of epoxy nanocomposites. Furthermore, we demonstrate that GO derived from pitch-based GFs can be an effective reinforcement as an alternative 2-D material for polymeric matrix, and present perspective to meet the requirements of light weight and strong mechanical properties for automotive and aerospace applications [30,31].

2 Experimental

2.1 Materials

The pitch-based GFs (labeled as GF, model: XN-90-60S) were provided by Nippon Graphite Fiber Co., Ltd. Epoxy resin (EP, diglycidyl ether of bisphenol-A), with an epoxide equivalent weight of 185–190 g eq^{-1} at room temperature, was purchased from Kukdo Chemical Co., Korea. 4,4′-Diaminodiphenylmethane (DDM) was supplied by TCI Co., Japan. Potassium permanganate ($KMnO_4$) was purchased from Daejung Co., Ltd. Sulfuric acid (H_2SO_4, 98%), phosphoric acid (H_3PO_4, 85%), and hydrogen peroxide (H_2O_2, 30%) solution were purchased from Duksan Pure Chemicals Co., Korea.

2.2 Preparation of GF-derived GO

The synthesis procedure is shown in Figure 1(a). The as-received GFs were cut into fragments and then ground in a ball mill at 250 rpm for 4 h to obtain GF particles (GFPs). Oxidation was performed using the modified Hummer's method [32]. Then, 3 g of GFPs was added to a 500 mL three-necked round-bottom flask charged with a mixture of concentrated H_2SO_4 (360 mL) and H_3PO_4 (40 mL). Next, 21 g of $KMnO_4$ was slowly added to the flask, and the temperature of the solution was maintained at 0–4°C for 6 h before increasing it to 60°C for 18 h. The solution was poured into 2,000 mL of ice water, followed by dropwise addition of H_2O_2 until no new bubbles emerged. The solution was treated by the following steps: static precipitation for 24 h, centrifugation to remove most of the acid solution, and infiltration to remove the remaining acids. The final GO sample was obtained using the freeze-drying process, and 4.8 g of GO was collected to be used as a reinforcement.

2.3 Fabrication of EP/GO nanocomposites

Figure 1(b) illustrates the fabrication process of EP/GO nanocomposites. A Fritsch planetary ball mill (Pulverisette 6, TMC) was employed to break up the agglomerates and enhance the dispersion of GO sheets. Without pretreatment of the samples, quantitative GO, EP, and a moderate amount of acetone were added to the grinding bowl and mixed at a rotational speed of 200 rpm for 4 h. Notably, the rotational speed should not exceed 250 rpm because the GO structure would be destroyed under the high shear stress [33]. The mixture was then degassed at 80°C for 48 h to remove the solvent completely. DDM (20 wt% of EP) was then slowly added to the solution and mixed with a planetary mixer, followed by further degassing at 60°C for 30 min. The prepared EP/GO samples were cured by the following three steps: 110°C for 1 h, 140°C for 2 h, and 170°C for 1 h.

2.4 Characterization

X-ray diffraction (XRD; D2 Phaser, Bruker, Germany) was used to investigate the structure of the GO in the 2θ range of 4–60°. Fourier-transform infrared spectroscopy (FT-IR; Jasco PS-4000, JASCO, Japan) was used to obtain the infrared spectra of the GO. The qualities of the fillers before and after thermal oxidation were analyzed by Raman spectroscopy (Raman; LabRAM Revolution, HORIBA, Japan) equipped with a charge-coupled device detector. X-ray photoelectron spectroscopy (XPS; ESCA LAB MK-II, VG Scientific, UK) was conducted to analyze the surface chemistry of the GO. High-resolution scanning electron microscopy (HR-SEM;

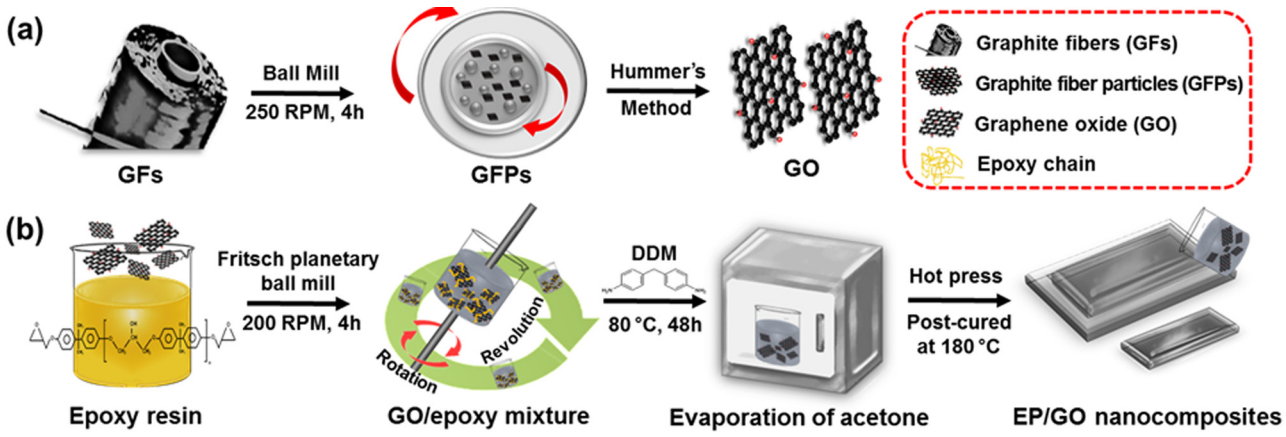

Figure 1: Schematic representation of EP/GO composites: (a) synthesis of GO derived from pitch-based GFs and (b) composite preparation process.

SU 8010, Hitachi, Japan) was used to observe the cross-section morphology of the prepared nanocomposites. Field-emission transmission electron microscopy (FE-TEM; JEM-2100F, JEOL, Japan) was used to examine the structure of the GO. The dynamic mechanical properties were measured using rectangular specimens with dimensions of 20 mm × 5 mm × 2 mm, held in a dual-cantilever clamp, using a dynamic mechanical analyzer (DMA; Q800, TA Instruments, USA).

The total surface free energy, which is the sum of London dispersive (γ^{L}) and specific components (γ^{SP}), can be calculated using the following equation [34]:

$$\gamma = \gamma^{L} + \gamma^{SP}, \tag{1}$$

where γ^{L} and γ^{SP} result from intermolecular interactions of London force of van der Waals attraction and the specific force, respectively.

According to Fowkes' suggestion [34], the surface free energy of a solid material can be examined by measuring the contact angle using the following geometric mean, known as the work of adhesion, W_A:

$$W_A = \gamma_L(1 + \cos\theta) \tag{2}$$

$$= 2\left(\sqrt{\gamma_S^L \cdot \gamma_L^L} + \sqrt{\gamma_S^{SP} \cdot \gamma_L^{SP}}\right), \tag{3}$$

where θ is the contact angle; subscripts L and S represent liquid and solid, respectively; superscripts L and SP represent London force and specific force, respectively. Equations (5–6) can then be transformed into the following equation:

$$\frac{\gamma_L(1 + \cos\theta)}{2\sqrt{\gamma_L^L}} = \sqrt{\gamma_S^{SP}}\left(\frac{\sqrt{\gamma_L^{SP}}}{\sqrt{\gamma_L^L}}\right) + \sqrt{\gamma_S^L} \tag{4}$$

According to this equation, a plot of $\frac{\gamma_L(1+\cos\theta)}{2\sqrt{\gamma_L^L}}$ against $\frac{\sqrt{\gamma_L^{SP}}}{\sqrt{\gamma_L^L}}$ should give a straight line, enabling easy calculation of the surface free energy [35].

The critical stress intensity factor (K_{IC}) of the EP/GO nanocomposites was examined *via* a three-point flexural test, which was performed using a universal test machine according to the standard ASTM E-399. A span-to-depth ratio of 4:1 and a crosshead speed of 1 mm min^{-1} were considered. The K_{IC} value of the cured epoxy and its nanocomposites was calculated using the following equations:

$$K_{IC} = \frac{PL}{bd^{3/2}} \cdot Y, \tag{5}$$

$$Y = \frac{3a/d^{1/2}[1.99 - (a/d)(1 - a/d)(2.15 - 3.93a/d + (2.7a^2/d^2)]}{2(1 + 2a/d)(1 - a/d)^{3/2}}, \tag{6}$$

where a, P, d, L, and b represent the crack length, critical load for crack propagation, thickness of specimen, length of the span, and the width of specimen, respectively.

The critical strain energy release rate (G_{IC}) of the epoxy and its nanocomposites was calculated using the following equation:

$$G_{IC} = \frac{(1 - \nu^2) \cdot K_{IC}^2}{E}, \tag{7}$$

where E is the Young's modulus obtained from the fracture test and ν is the Poisson's ratio for the nanocomposites (0.3). The flexural properties were tested with an Instron 1125 mechanical tester according to the standard ASTM D-790. To determine the mechanical properties,

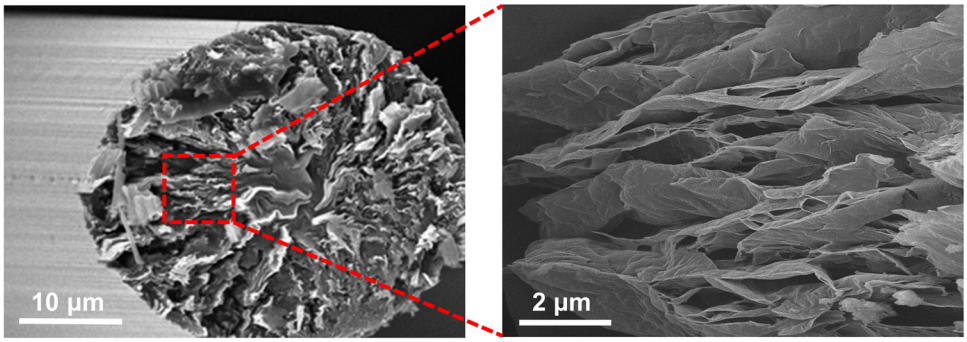

Figure 2: SEM images of the 2-D graphene nanosheets in the pitch-based GFs).

five experimental measurements were conducted for each specimen and the average value was obtained.

3 Results and discussion

3.1 Characterization of the GO

HR-SEM images of the GFs used in the study were observed to verify the presence of lots of stacked 2-D carbon sheets along with the long axis of the GF, as shown in Figure 2. Figure 3 displays the FT-IR spectra of the GF and GO derived from the GF. As shown in Figure 3(a), the FT-IR spectra of the GF demonstrated a small absorption peak at 3,380 cm^{-1} corresponding to hydroxyl groups (–OH). For the GO, new peaks were observed at 1,732 cm^{-1}, which can be attributed to stretching vibrations of the carboxylic groups (–COOH). The functional groups of the prepared GO are consistent with those reported in previous studies, demonstrating the feasibility of oxidation [36–38]. Photographs of GO suspension in water are shown in the inset of Figure 3(b). GO was homogeneously dispersed to generate a deep yellow-brown suspension. Figure 3(b) shows the TEM image of GO, exhibiting a typical 2-D nanosheet morphology with a particle size of approximately 2 μm. The grid can be clearly observed because of the superior transparency of the prepared GO. The XRD patterns of the GF and GO are shown in Figure 3(c). The pattern of the GF shows a typical graphite peak of (002) at 26.8°, corresponding to an interlayer d-spacing of 0.330 nm. In the case of GO, a new typical peak of (001) at 10.5° corresponding to a d-spacing of 0.84 nm appeared, indicating that a large degree of exfoliation occurred in the graphitic layers. This result confirmed that the stacked graphitic layers were completely exfoliated and converted into GO, which is in good agreement with the previous results of a typical structure of GO.

We employed Raman spectroscopy to observe the microstructural characteristics of the GF and GO. Basically, the Raman spectra of carbon nanomaterials present two peaks corresponding to the G- and D-bands at approximately 1,590 and 1,350 cm^{-1} due to the presence of sp^2 crystalline and sp^3 amorphous hybridized carbons, respectively [32,39]. As expected, two characteristic peaks in the GFs and

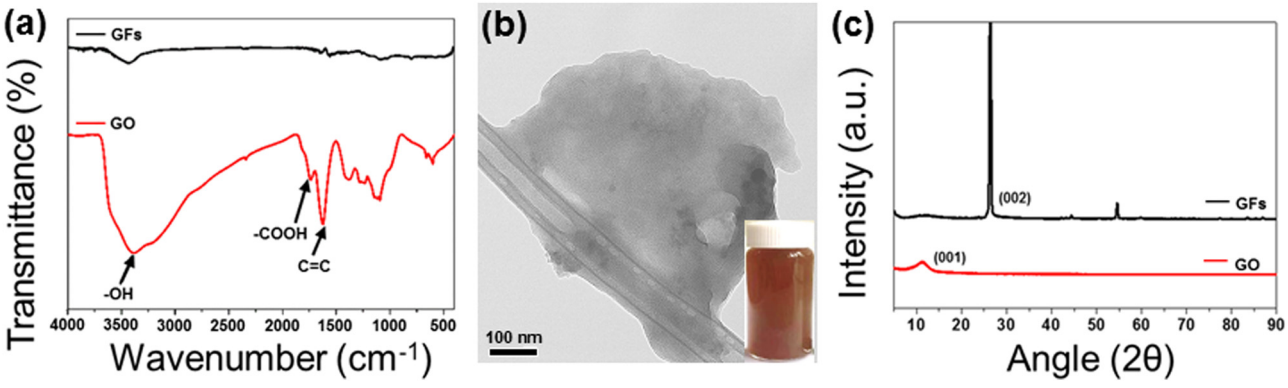

Figure 3: Characterization of GO: (a) FT-IR spectra of the GF and GO, (b) TEM image of GO (the inset: photographs of GO suspension in the water), and (c) XRD patterns of GF and GO.

GO were observed at 1,584 and 1,352 cm^{-1}, as shown in Figure 4(a). To investigate the degree of amorphous and crystalline phases, the integrated intensity ratio (I_D/I_G) from the D- and G-bands was calculated. The I_D/I_G increased from 0.45 (GF) to 1.08 (GO), indicating a decrease in the average size of the sp^2 graphene domains in GO compared to the GF.

XPS analysis was conducted to determine the surface chemical compositions and functional groups of the GO. In Figure 4(b), the two predominant characteristic peaks observed at 285.0 and 531.0 eV can be attributed to C1s and O1s core-level emissions, respectively. The carbon/oxygen (C/O) ratios were also calculated. The C/O ratio of the GFs was 6.14, which is mostly composed of carbon in the pristine GF, while the GO showed a much lower value of C/O ratio (1.13). To further confirm the surface functional groups of the GFs and GO, their high-resolution single-scan C1s spectra were deconvoluted. In Figure 4(c and d), the peaks of the GFs observed at 284.4 and 286.6 eV correspond to the C–C and C–O groups, respectively, indicating the presence of majorly conjugated sp^2 carbons and little oxygen. For the GO spectra, a broad peak was observed at 284.4 eV owing to an increase of full width at half maximum, resulting from the introduction of oxygen-functional groups. Moreover, the prominent peak at 289.2 eV corresponding to the carboxylic group (–COOH) was observed, indicating successful oxidation.

3.2 Interfacial properties of EP/GO nanocomposites

Surface free energy (γ) can strongly affect the wettability, adhesion, adsorption, and morphology of the components of composites. The London dispersion force, specific component force, and surface tension of the liquids are given in Table S1. The contact angles of the composites are shown in Table S2. Using the data provided in Tables S1 and S2, we calculated the surface free energies of the EP/GO, as plotted in Figure 5(a). The surface free energies of the EP/GO nanocomposites increased with increasing GO loading fractions. The EP/GO0.8 nanocomposites exhibited a surface free energy of 47.3 mJ m^{-2}, indicating that GO is compatible with EPs. In addition, the calculated values of W_A were gradually increased

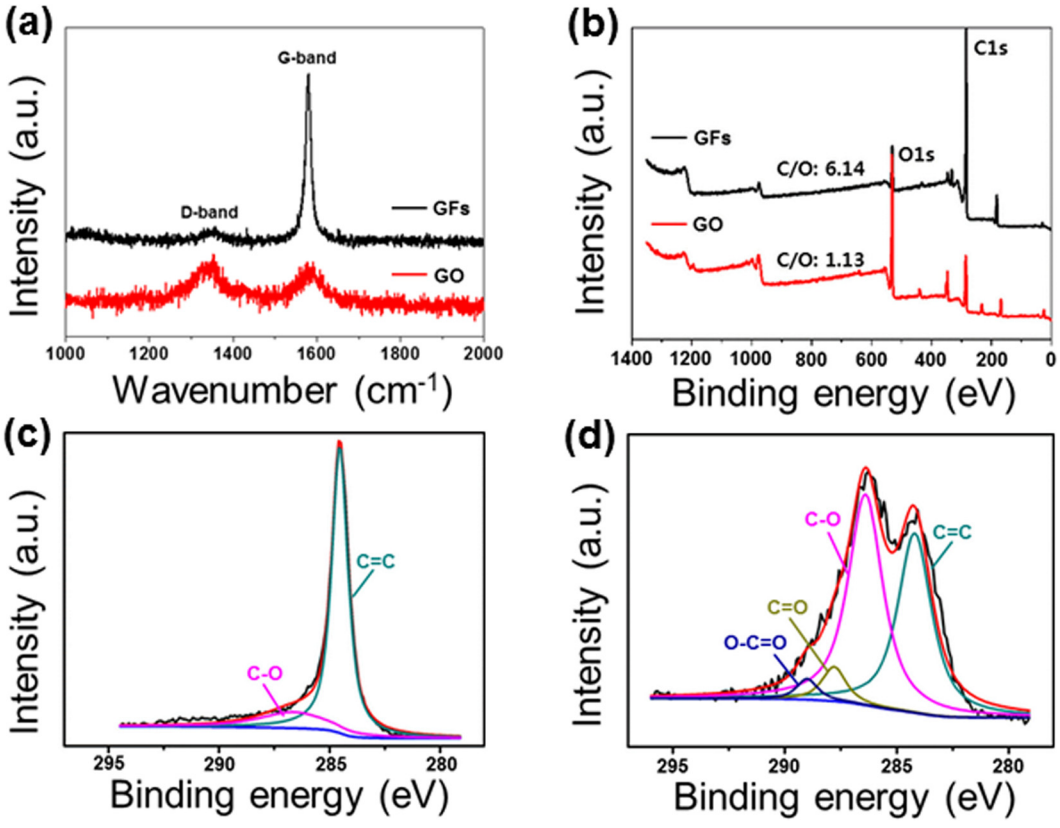

Figure 4: Characterization of GO: (a) Raman spectra of the GF and GO, (b) XPS survey spectra of the GF and GO, (c) C_{1s} spectra of the GF, and (d) C_{1s} spectra of the GO.

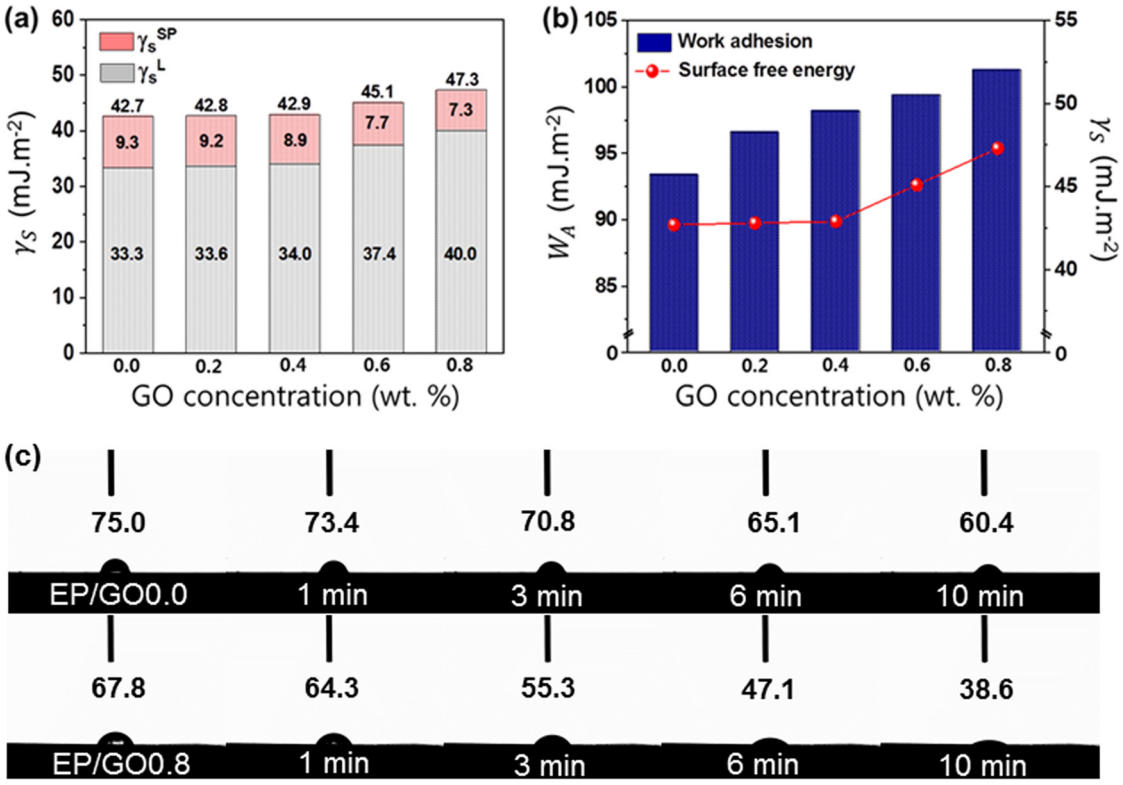

Figure 5: Interfacial behaviors of prepared EP/GO nanocomposites: (a) surface free energy, (b) work of adhesion, and (c) optical images of the wetting behavior of distilled water over time.

with an increase of the GO content (Figure 5(b)). Here, all the EP/GO nanocomposites exhibit good linearity for the relationship between the surface free energies and work adhesion, which clearly demonstrates enhanced interfacial adhesion [40,41]. We studied the wetting behavior of distilled water (carried out at 27°C for 10 min) acting on the nanocomposites in more detail. It can be seen from Figure 5(c) that the wetting behavior of the EP/GO0.0 nanocomposites was maintained at roughly 60.4° exhibited no obvious changes. By contrast, the wetting behavior of the EP/GO0.8 nanocomposite is seen to decrease rapidly and become saturated at around 38.6°. This decrease is due to the large number of carboxylic groups on the GO surface, from which water droplets can rapidly diffuse, thus providing an enhanced wettability for the nanocomposites.

3.3 Mechanical properties of EP/GO nanocomposites

The bending strength of the EP/GO nanocomposites increased up to 0.6 wt% by weight and then decreased at a higher GO content (Figure 6(a)). The bending strength of the epoxy nanocomposites reached 55.7 MPa in EP/GO0.6 nanocomposites, which is twice that of EP/GO0.0 nanocomposites (28.5 MPa). In addition, the Young's modulus (Figure 6(b)) showed a similar trend to the bending strength.

Normally, filler dispersion, interfacial interactions between the filler and polymer matrix, and the intrinsic characteristics of the filler are known to be three dominant factors affecting the performance of nanocomposites. In this work, since all the specimens were prepared through the ball-milling process, thereby ensuring good dispersion of the filler in the polymer matrix, the dispersion factor alone cannot account for enhanced mechanical properties. Meanwhile, the EP/GO nanocomposites exhibited superior interfacial interactions because abundant oxygen-functional groups were introduced onto the GO surface, as shown in Figure 5, which have strong affinity with the epoxy matrix. Thus, these results revealed that the perfect interfacial interaction between GO and the epoxy occurred, resulting in enhanced mechanical properties of the nanocomposites [42,43]. To further demonstrate the interfacial properties between the filler and the matrix, the flexural strength (σ) and flexural modulus (E_b) of the EP/GO nanocomposites with different GO loading amounts were also calculated, using the following equations (8) and (9) [44,45]:

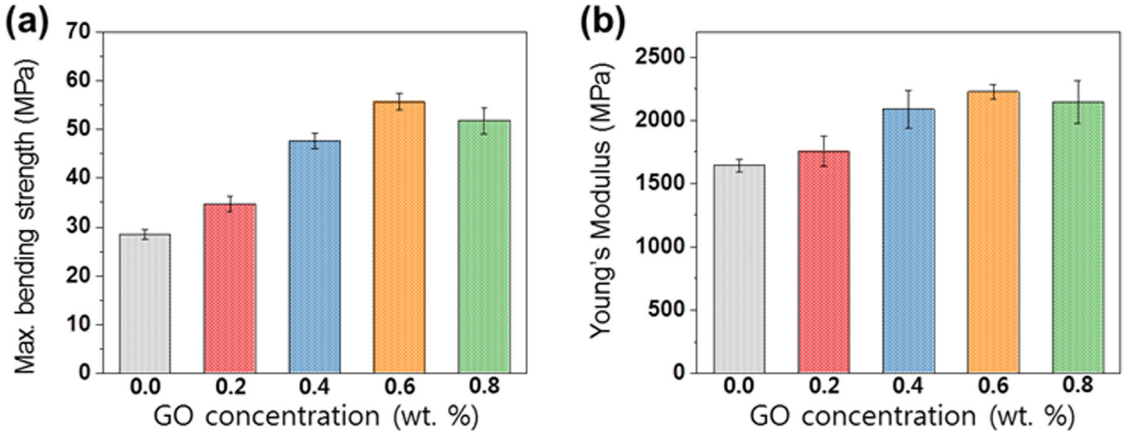

Figure 6: Mechanical properties of the EP/GO: (a) bending strength and (b) Young's modulus.

$$\sigma = \frac{3PL}{2bd^2}, \tag{8}$$

$$E_b = \frac{L^3}{4bd^3}\frac{\Delta P}{\Delta m}, \tag{9}$$

where P is the applied peak load, b is the sample width, d is the specimen thickness, L is the support span, ΔP is the variation in force at the linear portion, and Δm is the relative deflection variation.

Figure 7(a and b) shows the flexural strength and flexural modulus of EP/GO nanocomposites. With increasing GO loading fractions, the flexural strength gradually increased from 107 to 140 MPa. When the GO concentration exceeded 0.6% by weight, the flexural strength

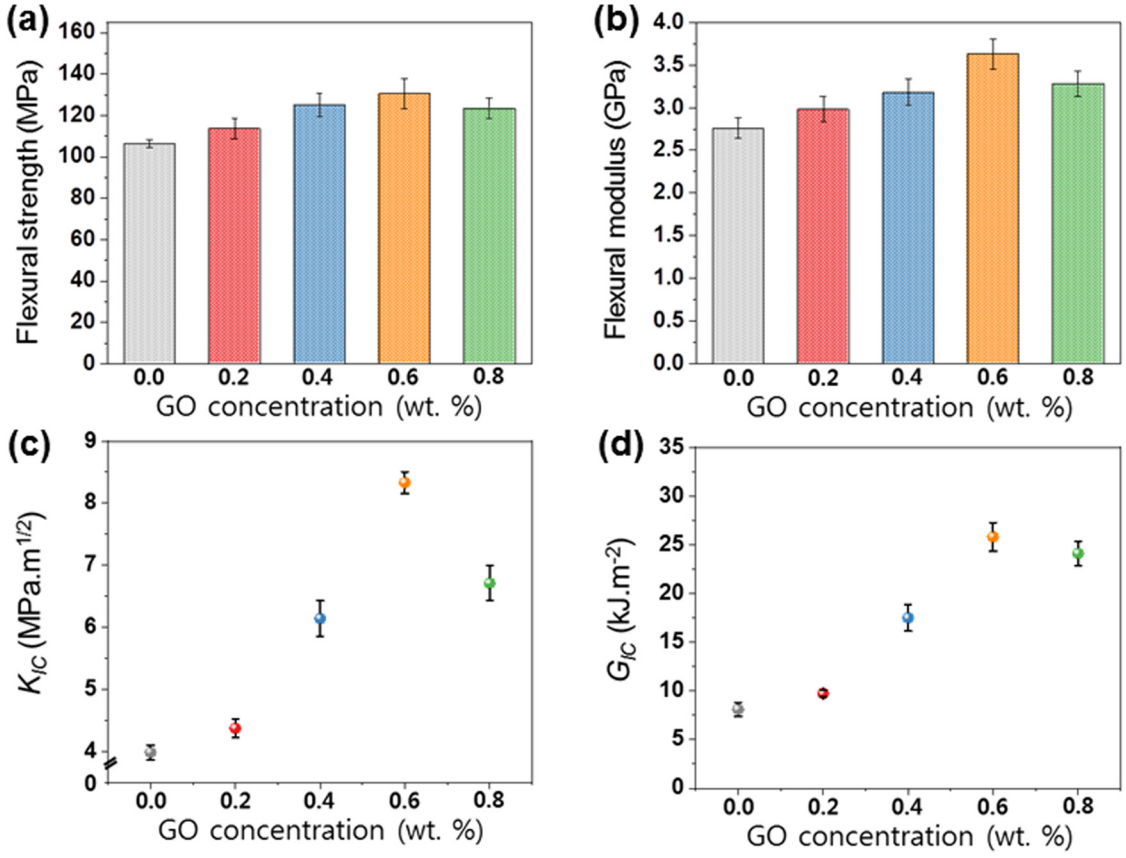

Figure 7: Mechanical properties of EP/GO nanocomposites: (a) flexural strength, (b) flexural modulus, (c) K_{IC}, and (d) G_{IC}.

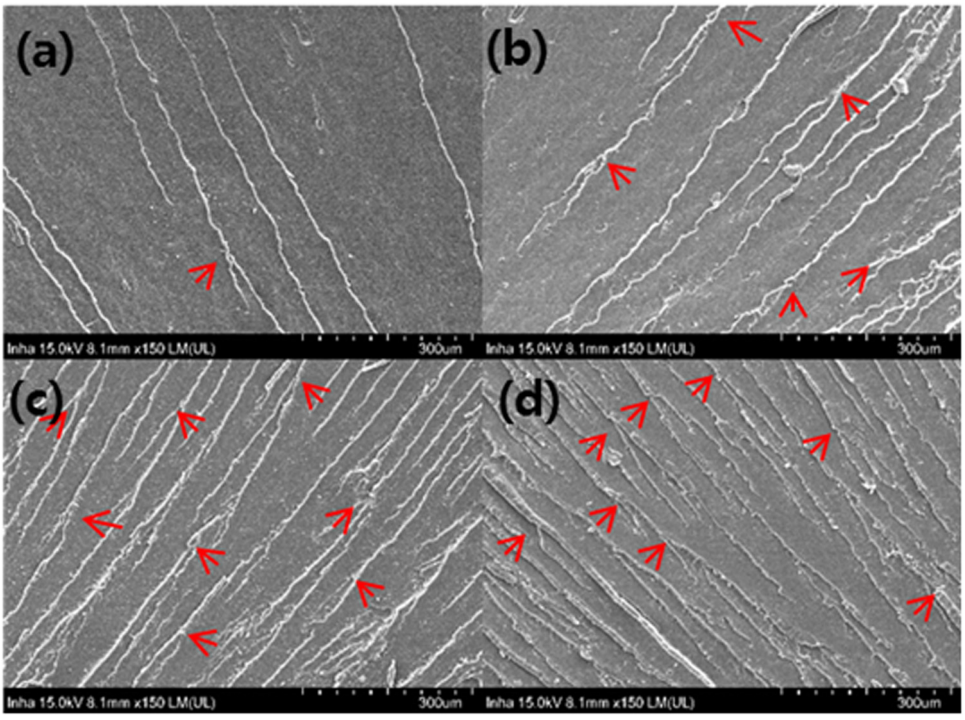

Figure 8: SEM images of the fracture surfaces: (a) EP/GO0.2, (b) EP/GO0.4, (c) EP/GO0.6, and (d) EP/GO0.8 nanocomposites.

decreased slightly. When the GO concentration exceeded 0.6% by weight, the flexural strength decreased slightly. The fracture toughness values were determined using the three-point bending tests, as shown in Figure 7(c and d). The results demonstrate that GO enhances both the fracture toughness (K_{IC}) and fracture energy (G_{IC}) of the prepared nanocomposites. The K_{IC} value of EP/GO0.6 nanocomposites increased by 109.3%; this enhancement can be attributed to the good dispersion of GO and thus the enhanced interfacial interactions within the epoxy matrix. Meanwhile, the EP/GO nanocomposites at higher fraction of GO (0.8% by weight) exhibited decreased K_{IC} value, probably due to the formation of aggregates. Correspondingly, the EP/GO nanocomposites exhibited the highest G_{IC} value in the EP/GO0.6 nanocomposites as well, demonstrating the best mechanical performances among the nanocomposites studied in the work.

It is well known that failure behaviors of nanocomposites are related to their structural integrity at both microscopic and macroscopic levels under external forces [44,46]. To reveal the failure behavior of the EP/GO nanocomposites, we observed their fracture surfaces using HR-SEM; the results are shown in Figure 8(a–d). With increasing GO loading fractions, the number of fatigue cracks increased and the surfaces became rougher. The equally distributed fatigue cracks on the fracture surfaces demonstrated homogeneously dispersed GO in an epoxy matrix. In EP/GO0.8 nanocomposites, the cracks were coarsened and pulled out, as shown in Figure 8(d), possibly due to the aggregation of the GO sheets. For the nanocomposites reinforced by a rigid additive, the plastic yielding of the epoxy matrix around the particles, subsequent void formations, and the interference of the rigid particles during crack propagation, including crack pinning and/or deflection, are considered as the main

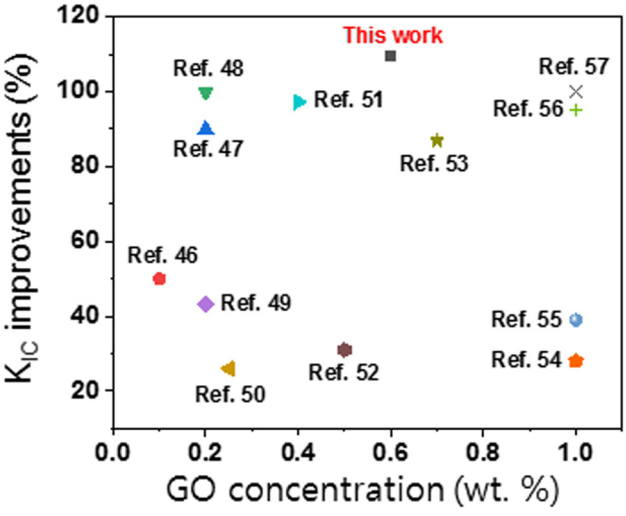

Figure 9: Comparison of the K_{IC} improvements of GO-loaded epoxy nanocomposites.

Table 1: Dynamic mechanical properties of neat epoxy and the EP/GO at 25°C

Specimen	Storage modulus (MPa)	T_g (°C)
EP	2.16	87.76
EP/GO0.2	2.19	88.33
EP/GO0.4	2.20	89.97
EP/GO0.6	2.23	90.38
EP/GO0.8	2.30	90.09

toughening mechanisms. In case of the EP/GO nanocomposites, crack deflection could act as the main toughening mechanism due to the increased number of cracks in the EP/GO nanocomposites [47].

In addition, the improvements in K_{IC} achieved by the addition of GO derived from pitch-based GFs in this study are compared with previously reported values for epoxy nanocomposites containing GO, as shown in Figure 9. It can be demonstrated that the prepared GO derived from pitch-based GFs plays an effective reinforcement for the K_{IC} improvements, resulting from enhanced interfacial interaction between the GO and epoxy matrix [48–59].

3.4 Thermophysical properties of EP/GO nanocomposites

DMA is used not only to determine the amount of elastic energy stored in the prepared composites and the energy dissipated during strain, but also to examine the glass transition temperature (T_g), which is the temperature at which sufficient vibration energy was accumulated to rearrange the crosslinked polymer chains inside the polymeric matrix. T_g is also known to be related to relaxation and is sensitive to structural transformations. The corresponding data of the temperature-dependent storage modulus and loss factor of the EP/GO nanocomposites are listed in Table 1. These data indicate that the homogenous dispersion of GO led to improved interfacial interaction between the GO sheets and the epoxy matrix, thereby substantially restricting the segmental movement of the epoxy chains and resulting in an enhanced storage modulus. The EP/GO nanocomposites exhibited a similar level of the dynamic storage moduli at the rubbery plateau area at the same temperature. We speculate that the presence of GO could play an important role in enhancing the dynamic storage modulus of the nanocomposites owing to the interfacial interaction between GO and the epoxy matrix. Moreover, the EP/GO nanocomposites exhibited higher T_g values than that of EP nanocomposites. The GO sheets served as anchor points among polymer chains, which restricted their mobility and increased the T_g. The T_g values increased with increasing GO loading fractions, demonstrating the enhanced interfacial interaction. The increase in the T_g value was not significant because the addition of a filler may reduce the cross-linking density of the epoxy, thus decreasing T_g [60].

4 Conclusion

In this study, GO was successfully synthesized using GFs as a precursor. The EP/GO nanocomposites at loadings less than 1% by weight were fabricated *via* ball-milling process. Presented detailed investigation of the mechanical and thermophysical properties of the EP/GO nanocomposites revealed that the values depend on the loading level of GO. In particular, when the GO loading was 0.6 wt%, the fracture toughness of the EP/GO nanocomposites exhibited a significant improvement of ~82% compared to that of EP nanocomposites. The fracture energies as well as the flexural strength and flexural modulus showed similar trends to the fracture toughness, demonstrating the effective toughness of GO. Moreover, the presence of GO improved the thermophysical properties of the epoxy matrix. These results can be attributed to the enhanced interfacial adhesion between the GO and the epoxy matrix, affecting the surface free energy and work adhesion. Collectively, these enhancements can be attributed to the good dispersion of GO, thereby enhancing the interfacial interactions between the GO and the epoxy matrix. Thus, the authors believe that the GF-derived GO in this work can be a promising candidate as a reinforcing material for improving the mechanical properties of nanocomposites in a wide range of applications.

Funding information: This work was supported by the Technology Innovation Program (or Industrial Strategic Technology Development Program – Development of Technology on materials and components) (20010106, Adhesives with low water permeability and low outgassing) funded by the Ministry of Trade, Industry & Energy (MOTIE, Korea) and supported by the Technological Innovation R&D Program (S2849653) funded by the Small and Medium Business Administration (SMBA, Korea).

Author contributions: All authors have accepted responsibility for the entire content of this manuscript and approved its submission.

Conflict of interest: The authors state no conflict of interest.

Data availability statement: The datasets generated during and/or analyzed during the current study are available in the Supplementary material on the journal website.

References

[1] Stankovich S, Dikin DA, Dommett GH, Kohlhaas KM, Zimney EJ, Stach EA, et al. Graphene-based composite materials. Nature. 2006;442:282–6.

[2] Geim AK. Graphene: status and prospects. Science. 2009;324:1530–4.

[3] Suk JW, Piner RD, An J, Ruoff RS. Mechanical properties of monolayer graphene oxide. ACS Nano. 2010;4:6557–64.

[4] Meyer JC, Geim AK, Katsnelson MI, Novoselov KS, Booth TJ, Roth S. The structure of suspended graphene sheets. Nature. 2007;446:60–3.

[5] Zhang Y, Heo YJ, Son YR, In I, An KH, Kim BJ, et al. Recent advanced thermal interfacial materials: a review of conducting mechanisms and parameters of carbon materials. Carbon. 2019;142:445–60.

[6] Yu T, Soomro SA, Huang F, Wei W, Wang B, Zhou Z, et al. Naturally or artificially constructed nanocellulose architectures for epoxy composites: a review. Nanotechnol Rev. 2020;9:1643–59.

[7] Liu C, Huang X, Wu YY, Deng X, Liu J, Zheng Z, et al. Review on the research progress of cement-based and geopolymer materials modified by graphene and graphene oxide. Nanotechnol Rev. 2020;9:155–69.

[8] Muñoz R, Gómez-Aleixandre C. Review of CVD synthesis of graphene. Chem Vap Depos. 2013;19:297–322.

[9] Lee HC, Liu WW, Chai SP, Mohamed AR, Aziz A, Khe CS, et al. Review of the synthesis, transfer, characterization and growth mechanisms of single and multilayer graphene. RSC Adv. 2017;7:15644–93.

[10] Kim SH, Rhee KY, Park SJ. Amine-terminated chain-grafted nanodiamond/epoxy nanocomposites as interfacial materials: Thermal conductivity and fracture resistance. Compos Pt B-Eng. 2020;192:107983.

[11] Chen G, Xu W, Zhu D. Recent advances in organic polymer thermoelectric composites. J Mater Chem C. 2017;5(18):4350–60.

[12] Dey A, Bajpai OP, Sikder AK, Chattopadhyay S, Khan MAS. Recent advances in CNT/graphene based thermoelectric polymer nanocomposite: a proficient move towards waste energy harvesting. Renew Sust Energ Rev. 2016;53:653–71.

[13] Jiao X, Qiu Y, Zhang L, Zhang X. Comparison of the characteristic properties of reduced graphene oxides synthesized from natural graphites with different graphitization degrees. RSC Adv. 2017;7(82):52337–44.

[14] Qiao Q, Liu C, Gao W, Huang L. Graphene oxide model with desirable structural and chemical properties. Carbon. 2019;143:566–77.

[15] Ikram R, Jan BM, Ahmad W. An overview of industrial scalable production of graphene oxide and analytical approaches for synthesis and characterization. J Mater Res Technol-JMRT. 2020;9:11587–610.

[16] Botas C, Álvarez P, Blanco C, Santamaría R, Granda M, Ares P, et al. The effect of the parent graphite on the structure of graphene oxide. Carbon. 2012;50:275–82.

[17] Brisebois PP, Siaj M. Harvesting graphene oxide–years 1859 to 2019: a review of its structure, synthesis, properties and exfoliation. J Mater Chem C. 2020;8:1517–47.

[18] Lee M, Lee J, Park SY, Min B, Kim B, In I. Production of graphene oxide from pitch-based carbon fiber. Sci Rep. 2015;5:1–10.

[19] Abdolkarimi-Mahabadi M, Manteghian M. Chemical oxidation of multi-walled carbon nanotube by sodium hypochlorite for production of graphene oxide nanosheets. Fuller Nanotub Carbon Nanostruct. 2015;23:860–4.

[20] Powell C, Beall GW. Graphene oxide and graphene from low grade coal: Synthesis, characterization and applications. Curr Opin Colloid Interface Sci. 2015;20:362–6.

[21] Das VK, Shifrina ZB, Bronstein LM. Graphene and graphene-like materials in biomass conversion: paving the way to the future. J Mater Chem A. 2017;5:25131–43.

[22] Kim SH, Park SJ. Effect of graphene oxide/graphitic nanofiber nanohybrids on interfacial properties and fracture toughness of carbon fibers-reinforced epoxy matrix composites. Compos Pt B-Eng. 2021;227:109387.

[23] Huang X. Fabrication and properties of carbon fibers. Materials. 2009;2:2369–403.

[24] Figueiredo JL, Bernardo CA, Baker RTK, Hüttinger KJ. Carbon fibers filaments and composites. Springer Sci Bus Media. 2013;177:1–236.

[25] Park SJ. History and structure of carbon fibers. Vol. 210. Singapore: Springer; 2018. p. 1–30.

[26] Yao SS, Jin FL, Rhee KY, Hui D, Park SJ. Recent advances in carbon-fiber-reinforced thermoplastic composites: a review. Compos Pt B-Eng. 2018;142:241–50.

[27] Kim SH, Park SJ, Rhee KY, Park SJ. Effects of ozonized carbon black on fracture and post-cracking toughness of carbon fiber-reinforced epoxy composites. Compos Pt B-Eng. 2019;177:107379.

[28] Peng J, Gao W, Gupta BK, Liu Z, Romero-Aburto R, Ge L, et al. Graphene quantum dots derived from carbon fibers. Nano Lett. 2012;12:844–9.

[29] Luo J, Cote LJ, Tung VC, Tan AT, Goins PE, Wu J, et al. Graphene oxide nanocolloids. J Am Chem Soc. 2010;132:17667–9.

[30] Yang X, Fan S, Li Y, Guo Y, Li Y, Ruan K, et al. Synchronously improved electromagnetic interference shielding and thermal conductivity for epoxy nanocomposites by constructing 3D copper nanowires/thermally annealed graphene aerogel framework. Compos Pt A-Appl Sci Manuf. 2020;128:105670.

[31] Song P, Liang C, Wang L, Qiu H, Gu H, Kong J, et al. Obviously improved electromagnetic interference shielding performances for epoxy composites via constructing honeycomb structural reduced graphene oxide. Compos Sci Technol. 2019;181:107698.

[32] Lee SY, Singh P, Mahajan RL. Role of oxygen functional groups for improved performance of graphene-silicone composites as a thermal interface material. Carbon. 2019;145:131–9.

[33] Wan YJ, Tang LC, Yan D, Zhao L, Li YB, Wu LB, et al. Improved dispersion and interface in the graphene/epoxy composites via a facile surfactant-assisted process. Compos Sci Technol. 2013;82:60–8.

[34] Fowkes FM. Determination of interfacial tensions, contact angles, and dispersion forces in surfaces by assuming additivity of intermolecular interactions in surfaces. J Phys Chem. 1962;66:382–2.

[35] Park SJ, Cho MS, Lee JR. Studies on the surface free energy of carbon–carbon composites: effect of filler addition on the ILSS of composites. J Colloid Interface Sci. 2000;226:60–4.
[36] Johra FT, Lee JW, Jung WG. Facile and safe graphene preparation on solution based platform. J Ind Eng Chem. 2014;20:2883–7.
[37] Dreyer DR, Todd AD, Bielawski CW. Harnessing the chemistry of graphene oxide. Chem Soc Rev. 2014;43:5288–301.
[38] Lee SY, Moore RB, Mahajan RL. An AI-assisted GO/rGO Janus film: fabrication and hygroscopic properties. Carbon. 2021;171:585–96.
[39] Malard LM, Pimenta MA, Dresselhaus G, Dresselhaus MS. Raman spectroscopy in graphene. Phys Rep. 2009;473:51–87.
[40] Behdinan K, Moradi-Dastjerdi R, Safaei B, Qin Z, Chu F, Hui D. Graphene and CNT impact on heat transfer response of nanocomposite cylinders. Nanotechnol Rev. 2020;9(1):41–52.
[41] Wu Q, Miao WS, Gao HJ, Hui D. Mechanical properties of nanomaterials: a review. Nanotechnol Rev. 2020;9(1):259–73.
[42] Keyte J, Pancholi K, Njuguna J. Recent developments in graphene oxide/epoxy carbon fiber-reinforced composites. Front Mater. 2019;6:224.
[43] Borooj MB, Shoushtari AM, Haji A, Sabet EN. Optimization of plasma treatment variables for the improvement of carbon fibres/epoxy composite performance by response surface methodology. Compos Sci Technol. 2016;128:215–21.
[44] Zhang Y, Rhee KY, Park SJ. Nanodiamond nanocluster-decorated graphene oxide/epoxy nanocomposites with enhanced mechanical behavior and thermal stability. Compos Pt B-Eng. 2017;114:111–20.
[45] Kim SH, Park SM, Park SJ. Role of dry ozonization of basalt fibers on interfacial properties and fracture toughness of epoxy matrix composites. Nanotechnol Rev. 2021;107:10–718.
[46] Zhang Y, Park SJ. Enhanced interfacial interaction by grafting carboxylated-macromolecular chains on nanodiamond surfaces for epoxy-based thermosets. J Polym Sci Pt B-Polym Phys. 2017;55:1890–8.
[47] Wang X, Jin J, Song M. An investigation of the mechanism of graphene toughening epoxy. Carbon. 2013;65:324–33.
[48] Galpaya D, Wang M, George G, Motta N, Waclawik E, Yan C. Preparation of graphene oxide/epoxy nanocomposites with significantly improved mechanical properties. J Appl Phys. 2014;116(5):053518.
[49] Wang TT, Huang P, Li YQ, Hu N, Fu SY. Epoxy nanocomposites significantly toughened by both poly (sulfone) and graphene oxide. Compos Commun. 2019;14:55–60.
[50] Chhetri S, Adak NC, Samanta P, Murmu NC, Kuila T. Functionalized reduced graphene oxide/epoxy composites with enhanced mechanical properties and thermal stability. Polym Test. 2017;63:1–11.
[51] Li Z, Wang R, Young RJ, Deng L, Yang F, Hao L, et al. Control of the functionality of graphene oxide for its application in epoxy nanocomposites. Polymer. 2013;54(23):6437–46.
[52] Wan YJ, Tang LC, Gong LX, Yan D, Li YB, Wu LB, et al. Grafting of epoxy chains onto graphene oxide for epoxy composites with improved mechanical and thermal properties. Carbon. 2014;69:467–80.
[53] Konnola R, Joji J, Parameswaranpillai J, Joseph K. Structure and thermo-mechanical properties of CTBN-grafted-GO modified epoxy/DDS composites. RSC Adv. 2015;5(76):61775–86.
[54] Katti P, Kundan KV, Kumar S, Bose S. Improved mechanical properties through engineering the interface by poly (ether ether ketone) grafted graphene oxide in epoxy based nanocomposites. Polymer. 2017;122:184–93.
[55] Sahu M, Raichur AM. Toughening of high performance tetrafunctional epoxy with poly (allyl amine) grafted graphene oxide. Compos B-Eng. 2019;168:15–24.
[56] Wazalwar R, Tripathi N, Raichur AM. Mechanical and curing behavior of epoxy composites reinforced with polystyrene-graphene oxide (PS-GO) core-shell particles. Compos C Open Access. 2021;5:100128.
[57] Shokrieh MM, Ghoreishi SM, Esmkhani M, Zhao Z. Effects of graphene nanoplatelets and graphene nanosheets on fracture toughness of epoxy nanocomposites. Fatigue Fract Eng Mater Struct. 2014;37(10):1116–23.
[58] Kang WS, Rhee KY, Park SJ. Influence of surface energetics of graphene oxide on fracture toughness of epoxy nanocomposites. Compos B-Eng. 2017;114:175–83.
[59] Bortz DR, Heras EG, Martin-Gullon I. Impressive fatigue life and fracture toughness improvements in graphene oxide/epoxy composites. Macromolecules. 2012;45(1):238–45.
[60] Zhang Y, Wang Y, Yu J, Chen L, Zhu J, Hu Z. Tuning the interface of graphene platelets/epoxy composites by the covalent grafting of polybenzimidazole. Polymer. 2014;55:4990–5000.